*energies*

MDPI

*Article*

# SiC and FeCrAl as Potential Cladding Materials for APR-1400 Neutronic Analysis

**Mohammad Alrwashdeh and Saeed A. Alameri ***

Emirates Nuclear Technology Center (ENTC), Department of Nuclear Engineering, Khalifa University of Science and Technology, Abu Dhabi P.O. Box 127788, United Arab Emirates; mohammad.alrwashdeh@ku.ac.ae
* Correspondence: saeed.alameri@ku.ac.ae

**Abstract:** The aim of this study is to investigate the potential improvement of accident-tolerant fuels in pressurized water reactors for replacing existing reference zircaloy (Zr) fuel-cladding systems. Three main strategies for improving accident-tolerant fuels are investigated: enhancement of the present state-of-the-art zirconium fuel-cladding system to improve oxidation resistance, replacement of the current referenced fuel-cladding system material with an alternative high-performance oxidation-resistant cladding, and replacement of the current fuel with alternative fuel forms. This study focuses on a preliminary analysis of the neutronic behavior and properties of silicon carbide (SiC)-fuel and FeCrAl cladding systems, which provide a better safety margin as accident-tolerant fuel systems for pressurized water reactors. The typical physical behavior of both cladding systems is investigated to determine their general neutronic performance. The multiplication factor, thermal neutron flux spectrum, $^{239}$Pu inventory, pin power distribution, and radial power are analyzed and compared with those of a reference Zr fuel-cladding system. Furthermore, the effects of a burnable poison rod ($Gd_2O_3$) in different fuel assemblies are investigated. SiC cladding assemblies present a softer neutron spectrum and a lower linear power distribution compared with the conventional Zr-fuel-cladding system. Additionally, the SiC fuel-cladding system exhibits behaviors that are consistent with the neutronic behavior of conventional Zr fuel-cladding systems, thereby affording greater economic and safety improvements.

**Keywords:** light water reactor; nuclear fuel; cladding; SiC; FeCrAl



**Citation:** Alrwashdeh, M.; Alameri, S.A. SiC and FeCrAl as Potential Cladding Materials for APR-1400 Neutronic Analysis. *Energies* **2022**, *15*, 3772. https://doi.org/10.3390/en15103772

Academic Editor: Hiroshi Sekimoto

Received: 13 April 2022
Accepted: 18 May 2022
Published: 20 May 2022



## 1. Introduction

In conjunction with innovations in the design of pressurized water reactors, fuel material behavior is being enhanced to develop alternative candidates for fuel-cladding materials, i.e., accident-tolerant fuels (ATFs). The fundamental motivation for investigating ATF systems is twofold: first, significant improvements to the basic design of certain existing reactors may be hard to implement, second, even if design changes exist, further improvements in reactor safety might be introduced by applying "a combination of fuel system innovations along with operational and/or reactor design changes" [1]. As reported by Nuclear Energy Agency of the OECD (NEA) [2] the main types of fuel-cladding system designs were investigated are: SiC-based, enhanced zircaloy, coated zircaloy, and steel-based cladding.

Many ATF concepts have been proposed as fuels for LWRs. For example, the FeCrAl and Mo cladding of uranium oxide ($UO_2$) fuel developed by Los Alamos National Laboratory (LANL) in collaboration with Electric Power Research Institute (EPRI) ("Fiscal Year 2013 Annual Report International Nuclear Energy Research"). Another concept based on a fully ceramic microencapsulated (FCM) fuel in FeCrAl or SiC cladding was developed by Oak Ridge National Laboratory (ORNL) [3].The Pacific Northwest National Laboratory (PNNL) developed the innovative concept of triple-layer co-extruded U-Mo metal fuel. And $U_3Si_5$, $U_3Si_2$, $UB_2$ and $UB_4$ fuels in FeCrAl or Zircaloy cladding were developed

by Brookhaven National Laboratory (BNL) [4]. The selection of the proposed accident tolerant fuel should be able to improve fuel performance during operation life cycle. The thermal conductivity of ATF-fuels should be also higher than the commercial $UO_2$ light water reactor fuel. High thermal conductivity cladding material have significant potential advantages over typical oxide-based fuels, including higher burnup, less fission gas release, and improved overall reactor system safety. One intriguing method to produce high thermal conductivity fuels involves combining high thermal conductivity ATF cladding materials with $UO_2$ fuel to lower the operating temperature. This takes advantage of $UO_2$'s highly favorable radiation resistance at lower operating temperatures. For this, ATF can assist in improving and maintaining reactor fuel performance during normal and abnormal conditions. Table 1 shows the thermo-physical properties for various fuel forms [5].

**Table 1.** Properties of accident tolerant fuels [5].

| Property | Fuel Form | | | | |
|---|---|---|---|---|---|
| | $UO_2$ | FCM | U-10Mo | UN | $U_3Si_2$ |
| Thermal conductivity (W/m-K) | 4 | 19 | 37 | 20 | 15 |
| Heat Capacity (J/kg-K) | 300 | 230 | 145 | 230 | 250 |
| Melting temperature (°C) | 2840 | 2400 | 1150 | 2762 | 1660 |
| Uranium density (g/cm$^3$) | 9.5–10.8 | 1–2 | 16.9 | 13.5 | 11.3 |

Most of the current ongoing research and development for the ATF claddings are focusing on the disadvantages in the current widely used commercial claddings: "hydrogen production and reduced mechanical properties at high burnup and severe conditions" [6]. In general, the iron-based alloys potential candidates for the ATF claddings-fuel system include FeCrAl, nickel-rich SS, and austenitic stainless steel (SS). The zircaloy cladding surface coating materials candidates are Cr, and CrAl.

Since the 1960s, when it was proposed that SiC may be used as a coating layer for reactor fuel design, there has been interest in using SiC for fission nuclear power reactors. The use of SiC in high-temperature gas-cooled reactors yields favorable behavior by the material under irradiation and a high-temperature environment. Researchers have proposed using SiC as an additional coating to the reactor fuel in order to minimize any damage in high-temperature reactors [7], when there is a high concentration of steam in the reactor coolant [8]. The main benefit of using SiC as an alternative cladding is its ability in reducing the oxidation rate [9]. Studies that predict SiC behavior in commercial pressurized water reactor environments are scarce. SiC has been applied as an external coating layer for $UO_2$ fuel pellets in high-temperature reactors (HTRs) [10] "as a container-like casing for $UO_2$ pellets in pressurized water reactors" [11], and as a heterogeneous material embedded in the fuel matrix [12]. More investigations must be conducted because most studies pertaining to cladding and fuel interaction, coolant and cladding interaction, and cladding irradiation are in the early phases or have not been fully developed. A previous comparison study was carried out by [13] described the effect of utilizing various fuel cladding systems for A0-type APR-1400 fuel assembly, and the neutronics penalty associated with each type of the candidate materials.

A significant amount of research pertaining to SiC-coated fuel particles of HTRs has been performed. Among them, three studies can be considered more important than the others. First, the earliest review performed by Price [14] presents the properties and structural behavior of SiC fuel coatings under irradiation conditions. A second outstanding review is the CEGA report [15], which provides a quantitative background regarding both the mechanical and thermal behaviors of SiC fuel-coating material, as well as summarizes the SiC properties required for modeling and simulation. A third excellent review published in 2007 by Snead [16] represents a "handbook" for SiC fuel-coating material properties.

FeCrAl fuel-cladding system is a promising alternative cladding material [17–19]. Owing to its favorable thermomechanical properties, such as its thermal expansion coefficient [20], oxidation resistance [21], thermal conductivity, melting point, and interdiffusion

with zirconium [22], FeCrAl was selected as a potential alternative cladding material. In general, regardless of the neutronics penalty of the cladding material, the following properties must be considered when selecting them: thermal conductivity, thermal expansion, density, swelling, elastic and shear modulus, temperature decomposition, fracture strength, and hardness. Furthermore, the aluminum in ferritic stainless-steel materials (such as FeCrAl) produces an oxide layer that can reduce the oxidation rate under severe conditions [23]. Figure 1 presents a general overview of the degradation process in a pressurized water reactor core for both the zircaloy (Zr)-fuel system and the potential candidate for the ATF-cladding material system.

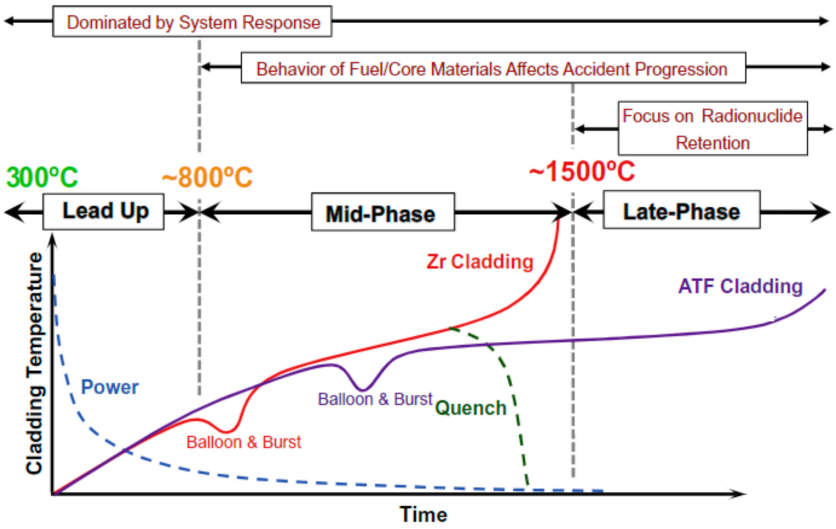


**Figure 1.** Pressurized water reactor accident progression scenario [20].

This paper focuses on preliminary neutronics analyses for both SiC and FeCrAl fuel cladding systems, for different APR-1400 fuel assembly designs, except assembly type A0 as it was analyzed in a previous work [13], and for the two-dimensional full reactor core. The neutronics parameters for the potential APR-1400 ATF cladding systems such as multiplication factor, neutron spectrum, linear power, and radial neutron flux were calculated and compared relative to the reference cladding, in particular, the neutronics penalty of adapting new fuel cladding system in the APR-1400 reactor core toward the End Of the Cycle (EOC).

## 2. Simulation Tools and Models

### *2.1. SiC and FeCrAl as Potential ATF Cladding*

In addition to the reference cladding material "zircaloy-4," the ceramic SiC and FeCrAl fuel-cladding systems were selected due to their higher corrosion resistance compared with the reference system [24]. Furthermore, the SiC ceramic was selected owing to its excellent performance in coating TRISO particles in high-temperature reactors [25,26] and its ability to reduce the generation of hydrogen gas under abnormal operating conditions [27]. FeCrAl has been investigated as a replacement for the reference cladding material owing to its improved high-temperature steam oxidation, which affords less hydrogen generation [28] under severe operating conditions [20]. To better understand the material composition, density, and thermal neutron economic effect of each system, the component elements as well as their interaction with the thermal neutron properties of each cladding material are summarized in Table 2. This table presents the chemical compositions of the cladding materials, and thermal neutron absorption cross-sections for the reference and alternative cladding materials. Figure 2 shows energy-dependent cross sections for reference and alternative cladding materials.

**Table 2.** Composition of cladding materials [2,29–31].

| Cladding Material | Cross Section (Barn) | Thermal Conductivity (W/m-K) | Melting Point (°C) | Density (g/cm$^3$) | Composition (wt %) | | | | | | |
|---|---|---|---|---|---|---|---|---|---|---|---|
| | | | | | Zr | Sn | Fe | Cr | Si | C | Al |
| Zircaloy-4 | 0.19440 | 21.5 | 1848.0 | 6.57 | 97.58 | 1.1 | 0.1 | 1.1 | — | — | — |
| SiC | 0.08600 | 120 | 2730.0 | 2.58 | — | — | — | — | 70.08 | 29.92 | |
| FeCrAl | 4.43000 | 26.0 | 1500.0 | 7.10 | — | — | 75.0 | 20.0 | — | — | 5.0 |

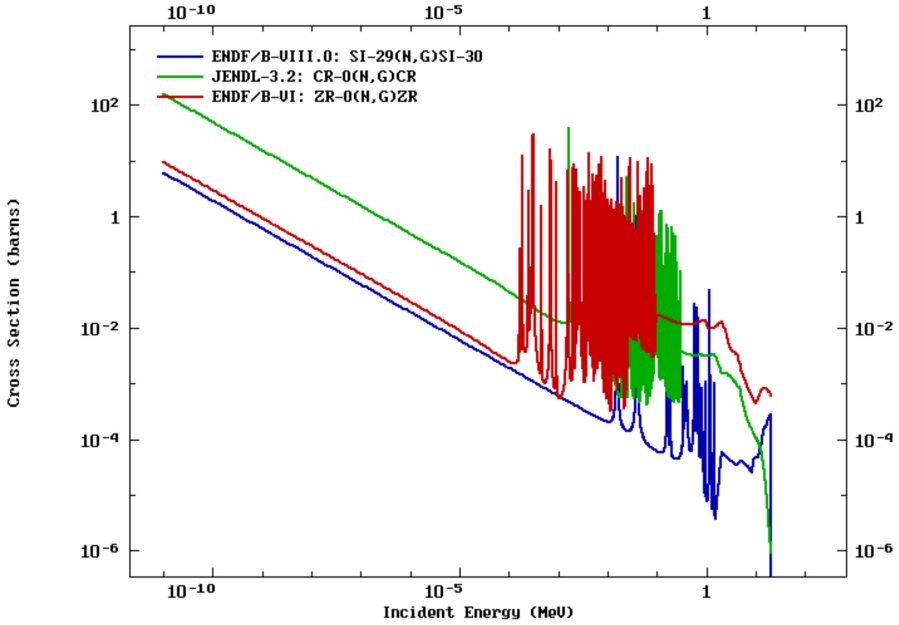


**Figure 2.** Microscopic absorption cross-section of the Zr, Si, and Cr.

### *2.2. APR-1400 Design Parameters*

The APR 1400 core contains 241 fuel assemblies, 93 control element assemblies, and 61 in-core instrument assemblies [32] with an active height of 3.810 m in a cylinder whose diameter is 3.647 m [33]. Each fuel assembly comprises 236 $UO_2$ rods with different enrichments. Most of the assemblies are mixed with gadolinium and five guide tubes [34]. Three types of normal assemblies without gadolinium were used, denoted as A0, B0, and C0. The other assemblies with $Gd_2O_3$ rods were denoted as B1, B2, C1, C2, and C3 [35]. Table 3 presents the specifications of the APR-1400 core design. Figure 3 shows the loading patterns of the fuel assemblies through the core.

**Table 3.** APR-1400 core design specifications.

| Item | Value |
|---|---|
| Number of fuel assemblies | 241 |
| Number of control assemblies | 93 |
| Number of fuel rod locations | 56,876 |
| Spacing between fuel assemblies, fuel rod surface to surface, cm | 0.549 |
| Total core area, m$^2$ | 10.433 |
| Core equivalent diameter, m | 3.647 |
| Total weight of zirconium alloy, kg | 29,511 |
| Fuel volume (including dishes), m$^3$ | 11.42 |
| Burnable absorber concentration ($Gd_2O_3$) | 8.0 w/o |

| | | | | | | | | |
|---|---|---|---|---|---|---|---|---|
| A0 | A0 | C2 | A0 | B1 | A0 | B2 | C2 | B0 |
| A0 | B0 | A0 | B2 | A0 | B2 | A0 | B2 | C0 |
| C2 | A0 | C2 | A0 | C1 | A0 | C2 | A0 | B0 |
| A0 | B2 | A0 | B2 | A0 | B2 | A0 | C1 | C0 |
| B0 | A0 | C1 | A0 | C2 | A0 | B1 | B0 | |
| A0 | B2 | A0 | B2 | A0 | B2 | C3 | C0 | |
| B2 | A0 | C2 | A0 | B1 | C3 | C0 | | |
| C2 | B2 | A0 | C1 | B0 | C0 | | | |
| B0 | C0 | B0 | C0 | | | | | |

**Figure 3.** First cycle fuel loading pattern.

### *2.3. Computation Tools*

Serpent code version 2.31 is a continuous energy-based code that utilizes the Monte Carlo method to perform both two- and three-dimensional reactor physics and burn-up calculations [36,37]. The built-in neutron evaluation routines can generate homogenized group constants for creating multi-group constants within a specific energy range specified by the end-user to perform full-core calculations. For a new concept of cladding system, the fuel geometry may be modified to overcome the neutronic penalty for newly applied materials. The full-core calculations performed for the fuel reactivity, thermal neutron flux, and group constants during the fuel lifecycle were obtained from neutron-transport simulations performed with the nuclear data library (ENDF/B-VII.1) [38], and enhanced nuclear data files for $^{233}$U and $^{239}$Pu [39,40]. Figure 4 presents a cross-sectional view of the different fuel assemblies as per Serpent 2.31 output model. The accompanying statical accuracy depends on the neutron history run, which is affected by the number of iterations of active cycle generations. Based on these considerations, the total cycles were set to 250 while skipping 50 cycles with particles per cycle set to $10^6$ neutrons for full core, $10^5$ for various fuel assemblies, and $10^4$ for fuel unit cell.

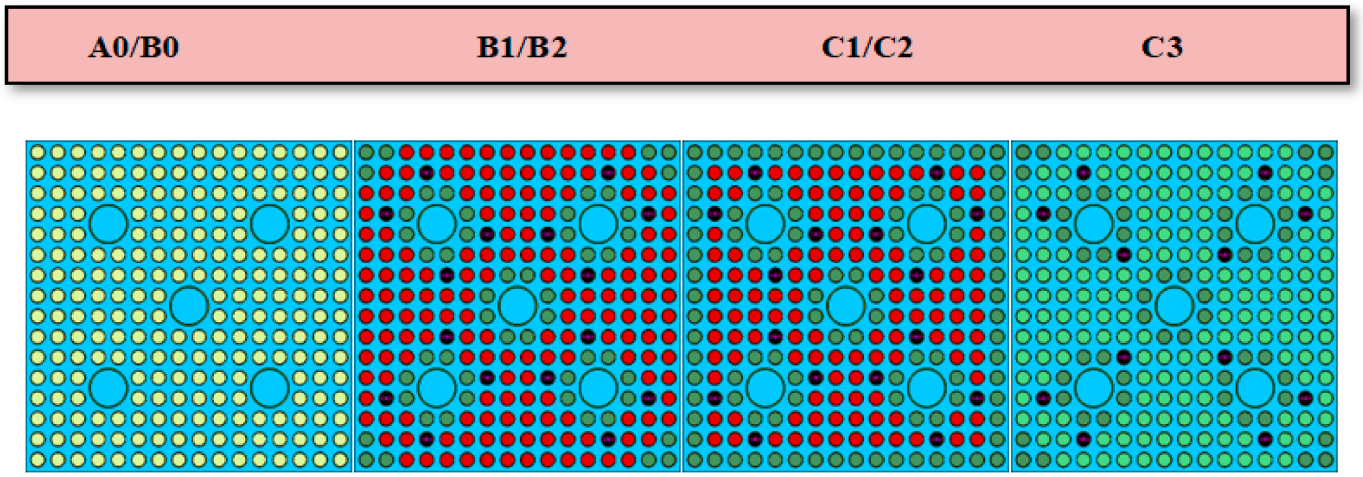


**Figure 4.** APR-1400 fuel assemblies cross sectional views.

## 3. Results and Discussion

### *3.1. Pin-Cell Calculations*

In this study, the applied pin-cell fuel enrichments were 1.68, 3.14, and 2.64 wt% with an exterior fuel pellet radius of 4.095 mm, helium gap of 85.0 μm, and cladding thickness of 570.0 μm [13]. Calculations for the fuel pin-cell model were performed using the collision estimator adopted in the Serpent 2.31 code [41]. The temperature for $UO_2$ was set to 900 K, whereas those for the cladding material and moderator were set to 600 and 580 K, respectively. Figure 5 presents the fuel pin-cell model generated using the Serpent 2.31 code.

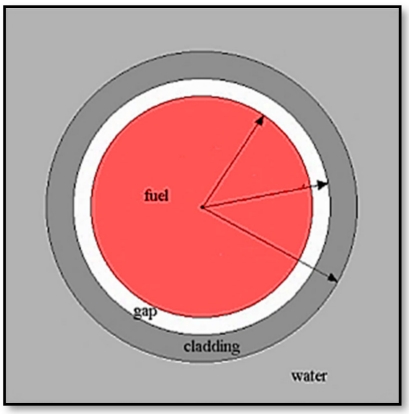


**Figure 5.** Fuel pin unit cell cross sectional view.

Figure 6 presents an example for evaluating the achievable effective full power equivalent operation days (EFPD) in the APR-1400 pin-cell model. To compare the reference material with both alternative claddings for different fuel enrichments, Figure 6 shows the effect of utilizing SiC and FeCrAl on the effective multiplication factor ($k_{eff}$). Table 4 summarizes the values of $k_{eff}$ for each fuel-cladding system at the Beginning Of the Cycle (BOC). As expected, high values of the absorption cross-section in FeCrAl cladding reduced the $k_{eff}$ values during the cycle, whereas the smaller absorption cross-section in SiC cladding caused an increase in the thermal neutrons inside the modeled system, resulting in higher values of $k_{eff}$ through the fuel-cycle compared with the reference material.

**Table 4.** $k_{eff}$ values for different pin-cell enrichments for three cladding materials at BOC.

| Fuel Enrichment (wt %) | $k_{eff,\ zircaloy}$ | $k_{eff,\ SiC}$ | $k_{eff,\ FeCrAl}$ |
|---|---|---|---|
| **1.68** | 1.16109 ± 0.00014 | 1.16940 ± 0.00013 | 1.02394 ± 0.00016 |
| **2.64** | 1.24543 ± 0.00014 | 1.25412 ± 0.00013 | 1.12104 ± 0.00014 |
| **3.14** | 1.31111 ± 0.00013 | 1.31928 ± 0.00013 | 1.19964 ± 0.00014 |

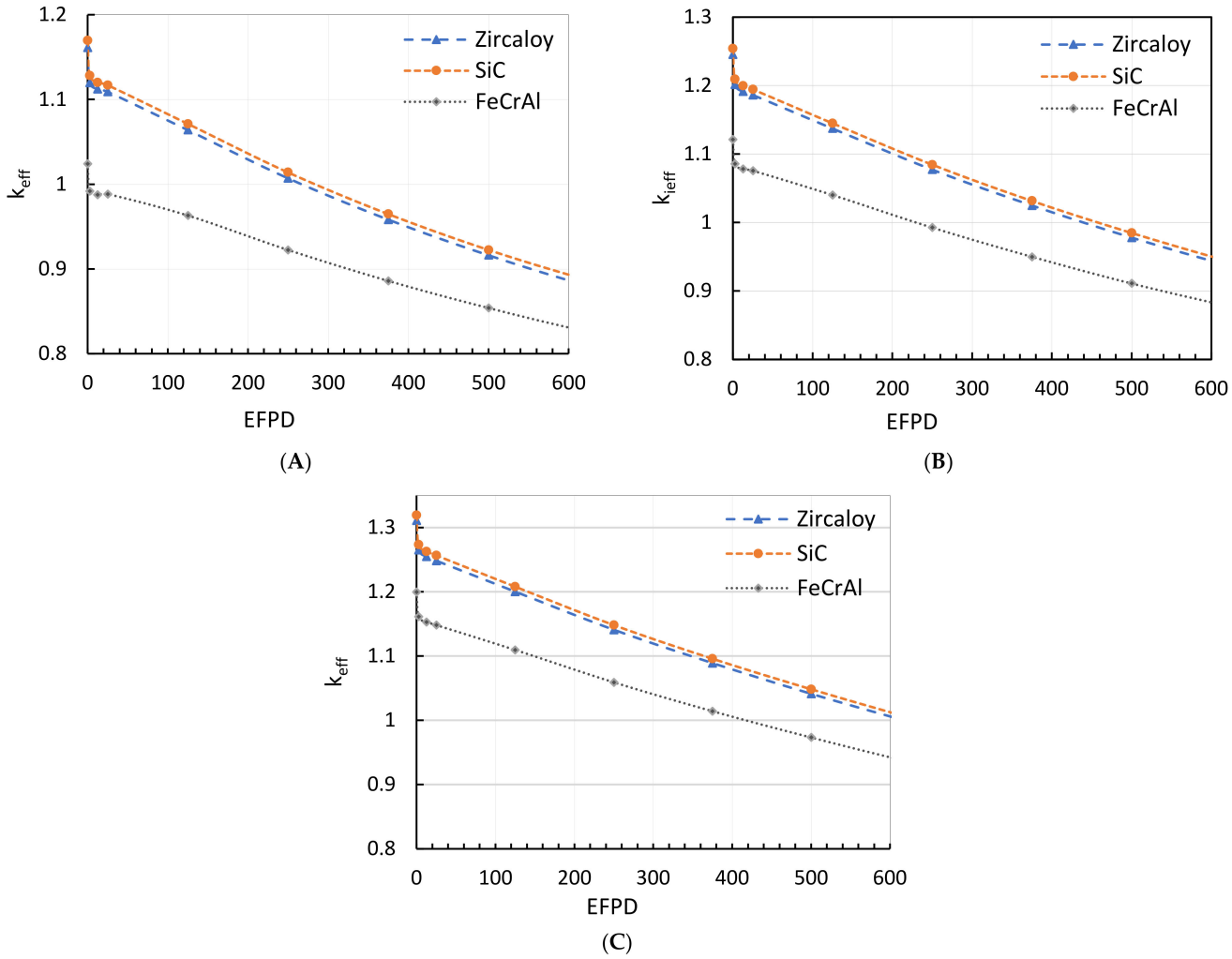


**Figure 6.** Unit cell effective multiplication factor versus EFPDs for the three cladding materials with different enrichments (**A**) 1.68 wt % (**B**) 2.64 wt %(**C**) 3.14 wt %.

Spectral hardening in the thermal energy region for both types of alternative cladding (SiC and FeCrAl) materials were investigated. Figure 7 shows the normalized flux spectra for the different fuel-cladding systems. Precisely, the thermal region of the neutron spectra was evaluated across a plane vertical to the pin-cell axial direction (fuel, cladding, and moderator). As presents in Table 2 and Figure 7, the FeCrAl cladding-fuel system exhibited larger thermal-neutron-absorbing cross-sections. Consequently, neutron spectrum hardening in the FeCrAl material is expected. The SiC cladding material has a smaller thermal neutron-absorbing cross-section compared with FeCrAl and Zr, which results in a high inventory of thermal neutrons and softening of the neutron spectrum.

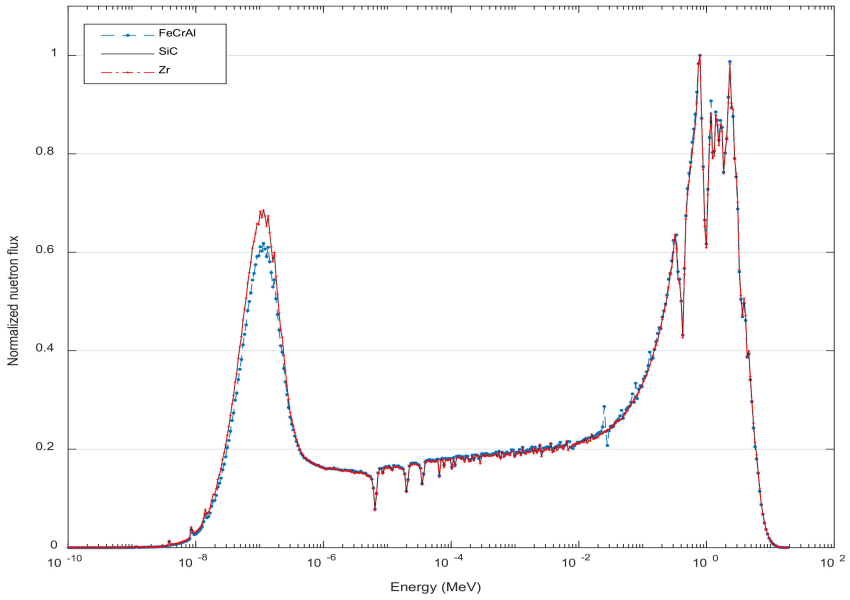


**Figure 7.** Normalized flux for different fuel−cladding materials.

### *3.2. Lattice Calculation*

Neutronic analyses were performed on the APR-1400 reactor fuel assemblies. Eight types of fuel assemblies were required to perform these analyses, as presented in Figure 4. In this study, the fuel enrichment and cladding thickness remained unchanged, as in the reference fuel-clad system. Figure 8 shows that the curves of the B0 assembly exhibited the same tendency as a function of burnup, whereas the higher-absorption cross-section of FeCrAl resulted into lower values of $k_{eff}$. At BOC, the $k_{eff}$ values for the Zr and SiC cladding systems were similar (i.e., 1.23772 $\pm$ 0.00011 and 1.24733 $\pm$ 0.00011, respectively) and substantially lower than those for the FeCrAl cladding (1.12775 $\pm$ 0.00012). The maximum reactivity differences at the BOC between the reference Zr and each of the SiC and FeCrAl were approximately 770.0 and −9751.0 pcm, respectively. Furthermore, fuel assemblies B1, B2, C1, C2, and C3 were modeled by inserting 16 gadolinium rods in each assembly except for C3 (12 were inserted), as shown in Figure 4.

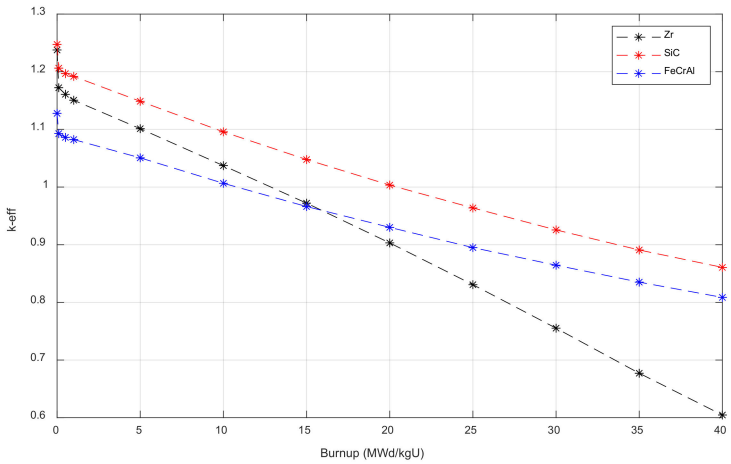


**Figure 8.** B0 effective multiplication factor versus burnup days for the three cladding materials.

Gadolinium-type assemblies have been used to reduce excess reactivity in reactor core designs. In general, two types of commercially available gadolinium rods are used in conventional light-water reactors: low and high wt% gadolinium. Currently, those with a high wt% are more widely used owing to their greater ability in reducing thermal

conductivity and their long-lasting reactivity suppression. The effect of the length-to-diameter ratio [42] can be significant at the BOC, particularly for rods with a low gadolinium wt%, whereas rods with a high gadolinium wt% are more efficient at the Middle Of the Cycle (MOC) as it can suppress the excess reactivity until 15 GWd/MTU. After this point, the effect of low or high wt% gadolinium is negligible.

The effect of the gadolinium rods is shown in Figure 9. It was evident that the gadolinium rods affected the $k_{eff}$ at the early steps of the fuel lifecycle. Similar trends were observed for the Zr and SiC fuel-cladding systems for the B2, C1, and C3 fuel assemblies. However, the high-absorption cross-section of FeCrAl resulted in a significantly suppressed fuel reactivity during the lifecycle.

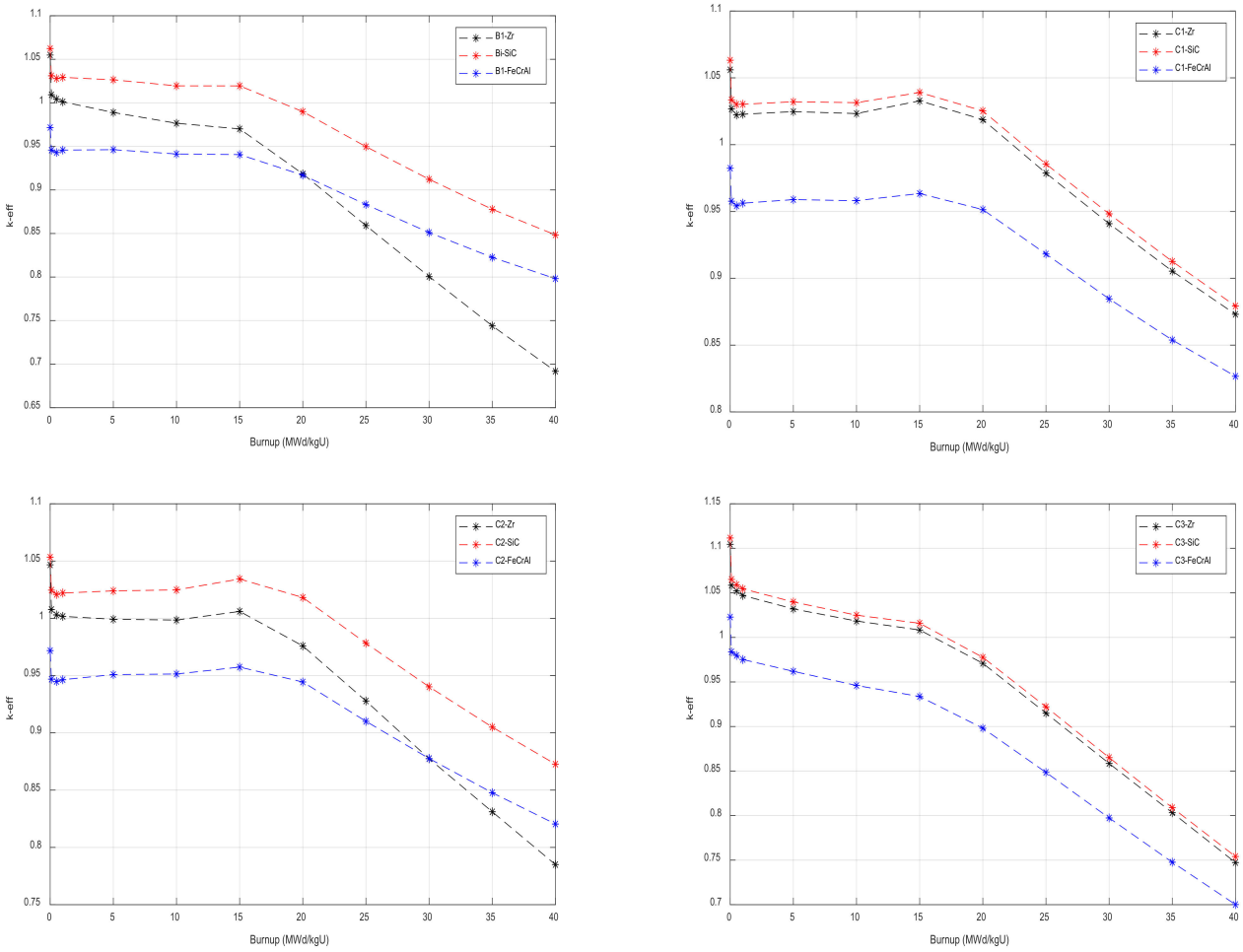


**Figure 9.** Effective multiplication factor versus burnup days for different fuel assemblies with Gd-rods.

Fuel assembly pin power distribution is an important output in neutronics safety analysis because it can be used to reduce the power-peaking factor and highlights the restricting fuel rod [43], i.e., the fuel rod with the highest heat flux at the cladding surface or the fuel rod with the highest fuel centerline temperature. It is also important to see if the distribution varies with time. In Figure 10, linear power distribution at the BOC of each pin of the specified fuel assemblies. The results were obtained and presented using the Serpent 2.31 code to simulate radial thermal neutron reaction rate and density distributions. The average linear powers for the B1-zircaloy, B1-SiC, and B1-FeCrAl assemblies were 186.68, 185.93, and 171.81 W/cm, respectively. By contrast, the linear power of the burnable absorber rod positions in the B1 and C1 fuel assemblies was approximately 37 to 39 W/cm for all types of fuel cladding. Additionally, the fuel rods nearest to the guide tube indicated

linear powers greater than those of the remaining fuels. More thermalized neutrons migrated from the moderator region to the fuel area. Conversely, the linear power was much lower in the burnable absorber rods and surrounding rods than in the normal fuel rods due to the large absorption cross-section of material in these rods.

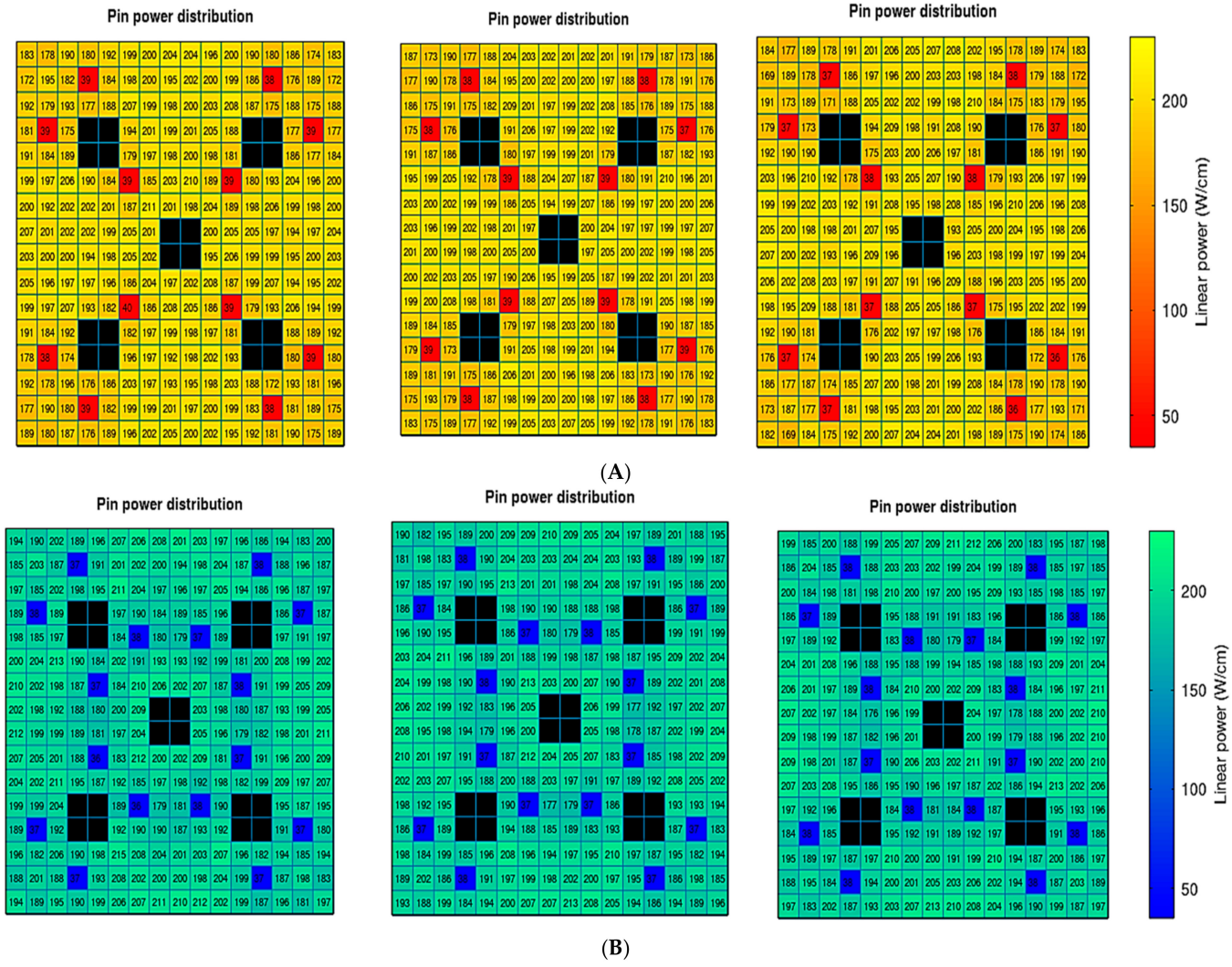


**Figure 10.** Power profile at BOC for B1 and C1 assemblies type for different fuel cladding systems. (**A**) B1−zircaloy, B1−SiC, and B1−FeCrAl, respectively. (**B**) C1−zircaloy, C1−SiC, and C1−FeCrAl, respectively.

The neutron flux was examined in the reactor design analysis because it is the main quantity that controls the fission reaction inside the core. The higher the neutron flux, the greater is the likelihood of a nuclear reaction occurring owing to the greater number of neutrons passing through an area per unit of time. In other words, the higher the thermal flux, the greater is the possibility of fission by U-235. As such, the neutron flux controls the power inside the core. Power is the integral of the product of flux, the energy released by a single fission, and the macroscopic fission cross-section over both space and energy. Figure 11 presents the normalized neutron spectrum for several types of fuel assemblies, namely B1, and C1, at the BOC, for all types of cladding materials.

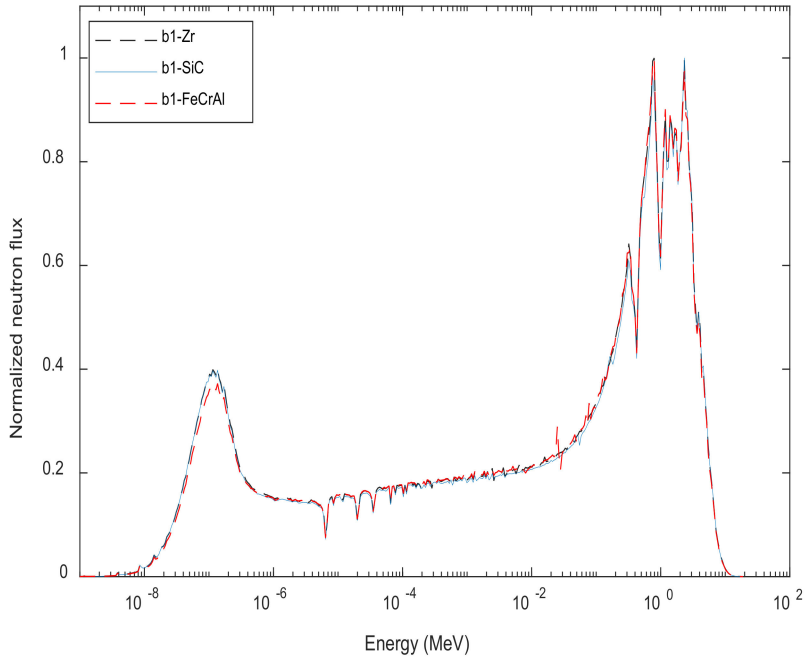


(**A**)

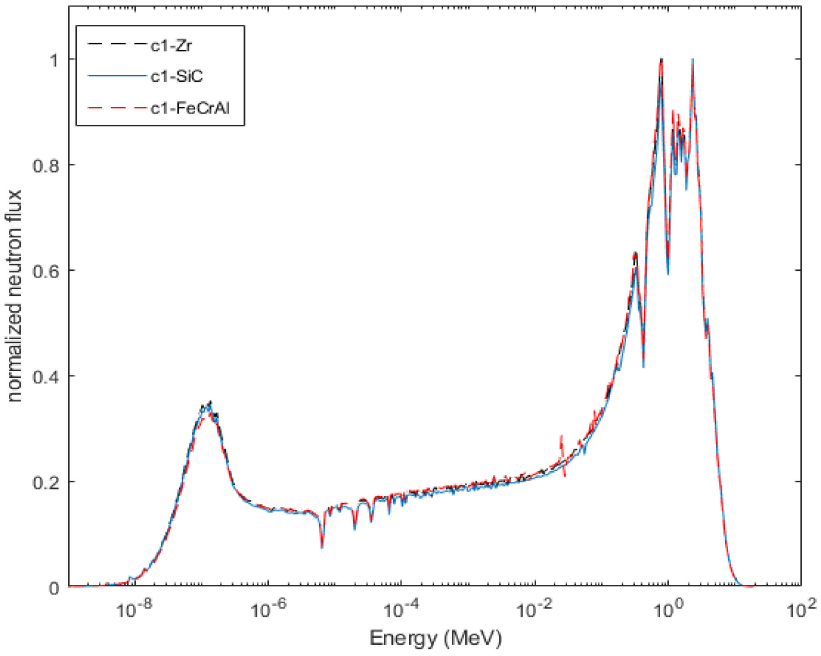


(**B**)

**Figure 11.** Normalized neutron flux distribution at BOC for different types of fuel assemblies (**A**) B1−zircaloy, B1−SiC, and B1−FeCrAl, (**B**) C1−zircaloy, C1−SiC, and C1−FeCrAl.

Neutron spectral hardening was investigated for various alternative cladding materials, by comparing alternative candidates with the reference Zr fuel-cladding system. As shown, the thermal neutron flux spectrum hardened as a result of the alternate cladding materials with higher neutron-absorbing cross-sections. The SiC cladding system, which had a smaller absorbing cross-section, was compared with the Zr cladding system, as presented in Table 2. The high-absorption cross-section of the FeCrAl cladding significantly affected the thermal neutron inventory, which was significantly lower than that of the other types of cladding systems (Zr and SiC). Consequently, the effect of the cross-section for cap-

turing thermal energy neutrons affected the neutron spectrum within the fuel assemblies containing Gd rods (i.e., B1 and C1).

Figure 12 shows the incremental changes in $^{239}$Pu inventory during fuel life cycle of the reference material and both types of alternative cladding (SiC and FeCrAl) materials for the modeled C1 fuel assembly with gadolinium rods. The amount of accumulative plutonium depended primarily on the fuel enrichment, fuel pin configuration, and type of fuel-cladding system. As shown in Figures 11 and 12, the material with a higher capturing rate of neutrons accumulated more plutonium. As expected, the hardening effect in the thermal region of the neutron spectrum was the greatest for the material with a higher-absorption cross-section or with fuel assemblies containing poisons such as gadolinium, as compared with the reference material (Zr). This was caused by an increase in the fast neutron population of the system because of the increased thermal neutron absorption in the steel-type cladding materials. Consequently, additional resonance capture of $^{238}$U occurred, which consequently increased plutonium generation. Hence, FeCrAl cladding resulted in a higher accumulation of plutonium as compared with Zr and SiC cladding.

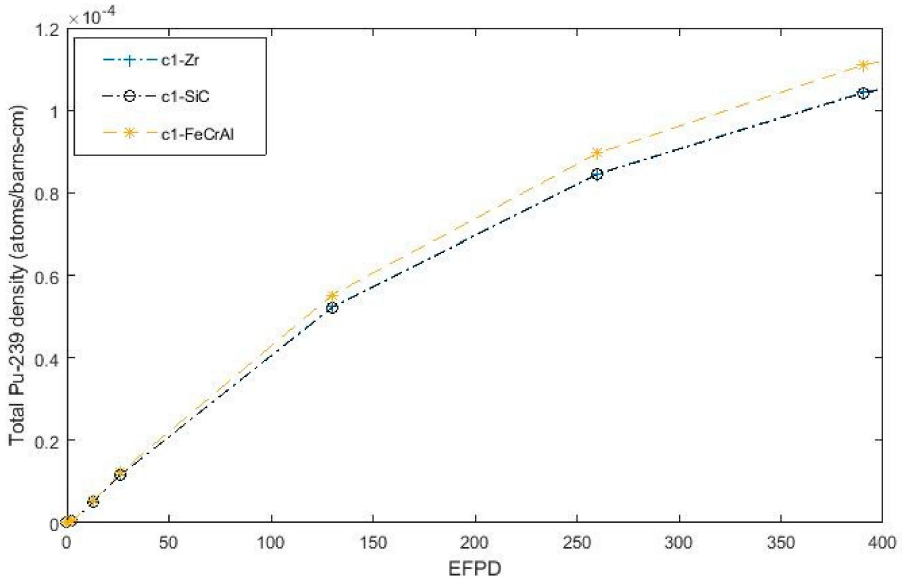


**Figure 12.** Pu−239 inventory for different types of fuel−cladding system. C1−zircaloy, C1−SiC, and C1−FeCrAl.

### *3.3. 2D Full Core Analysis*

For both types of cladding materials, a 2D APR-1400 full-core model was employed. Figure 13 presents the $k_{eff}$ toward the End Of the Cycle (EOC). As expected, the larger absorption cross-section of the FeCrAl cladding material resulted in a lower $k_{eff}$ value for the fuel system compared with the reference Zr and SiC fuel systems. This is favorable for the implementation of SiC as alternative cladding material instead of FeCrAl owing to the neutronics penalty of the latter one. In this research, some of the fuel assemblies contain Gd rods, as a result a significant decrease in the $k_{eff}$ at the BOC, due to the high absorption cross section of these types of rod material.

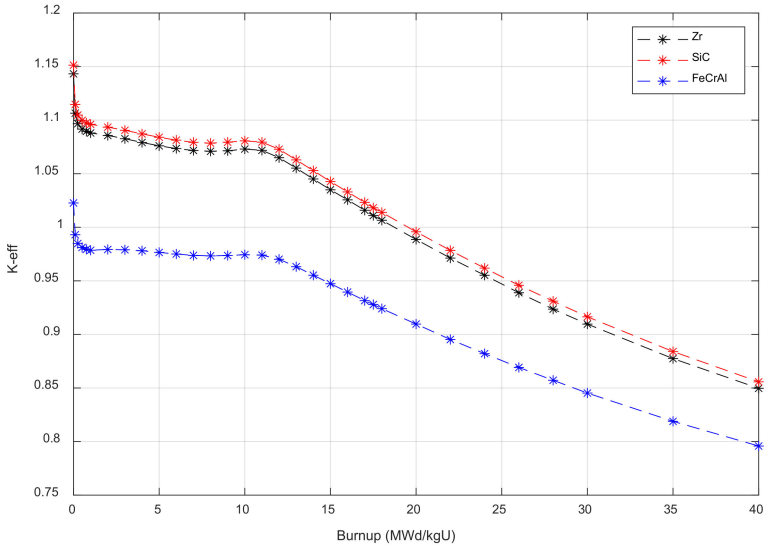


**Figure 13.** Effective multiplication factor versus burnup days for APR-1400 reactor core.

The excess of reactivity at BOC for the three different cladding materials results were as follows: 12,527 pcm for Zr, 13,142 pcm for SiC, and 2218 pcm for FeCrAl. As expected, the burnup reactivity swing between the BOC and EOC agreed well for Zr and SiC; however, it was much lower for FeCrAl as compared with that for Zr and SiC.

Figure 14 shows the initial 2D full-core calculations performed to evaluate the radial thermal neutron flux for both types of cladding materials at the BOC, MOC, and EOC. As observed, the thermal neutron flux was maximum at the center, and it decreased gradually toward the core boundary for both the Zr and SiC fuel-cladding systems. By contrast, the thermal flux was minimum at the center, and it increased toward the core boundaries in the FeCrAl fuel-cladding system. This happened because of the effect of the cladding material high-absorption cross sections on the hardening or softening of the neutron spectrum in a long-term operational light water reactor. Despite the reactivity penalty at the BOC, the FeCrAl cladding reduced the cycle length significantly because of its larger neutron-absorbing cross-section, even though its plutonium buildup was higher compared with the other cases. As a result, using FeCrAl cladding is not favorable in terms of the reactor core neutron economy, as present in Figure 13.

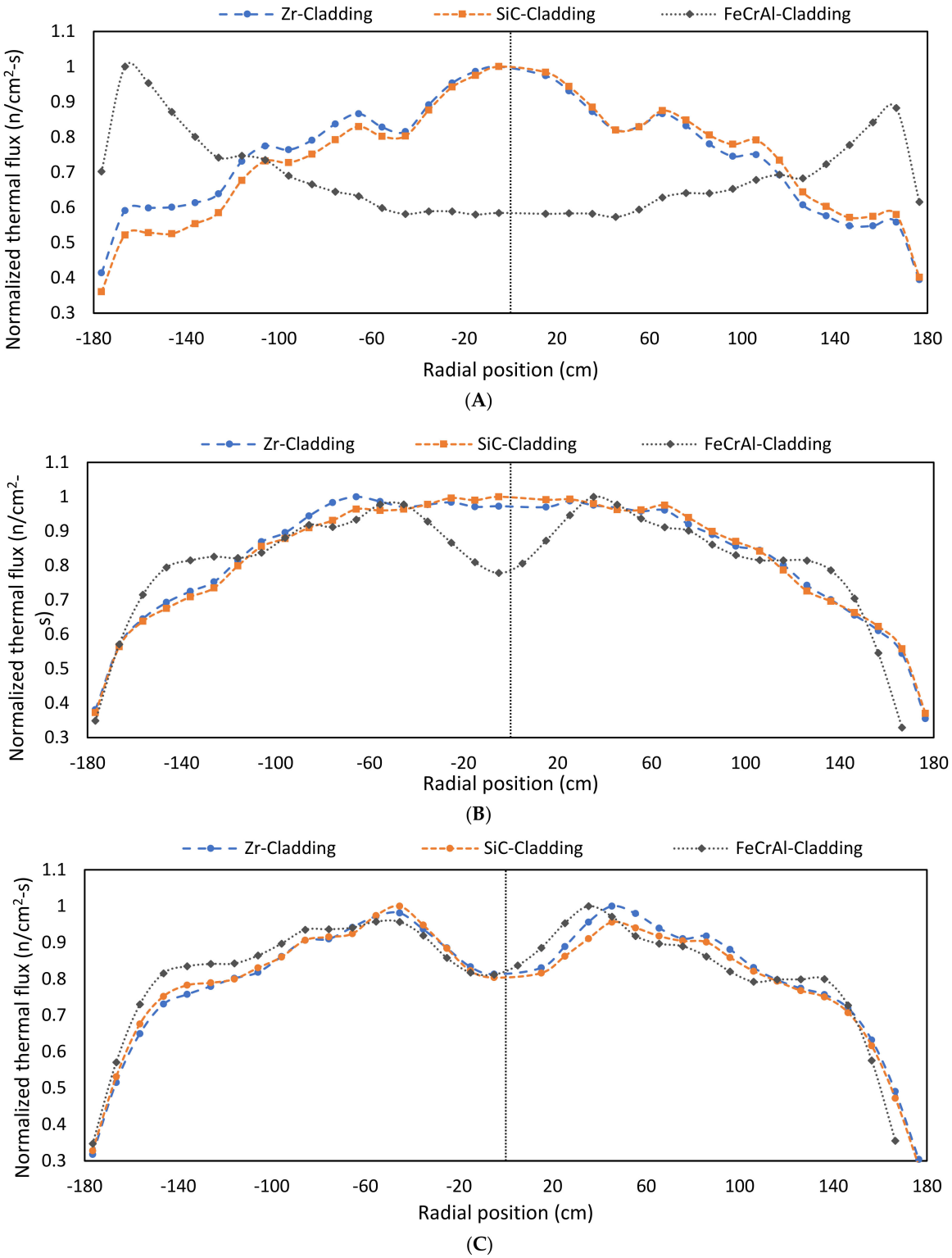


**Figure 14.** Radial power profile for three types of cladding materials at (**A**) BOC, (**B**) MOC, and (**C**) EOC, respectively.

## 4. Conclusions

Preliminary neutronics analyses were performed with respect to a reference Zr and alternative fuel-cladding systems for pin cells, fuel assemblies, and 2D full cores. Characteristic parameters of the alternative systems such as the flux spectrum, power distribution,

and multiplication factor were investigated and compared with those of the reference Zr fuel-cladding system.

As expected, for all the modeled cases, the high values of the absorption cross-section in FeCrAl cladding reduced the $k_{eff}$ values during the cycle. On the other hand, the smaller absorption cross-section in SiC cladding caused an increase in the thermal neutrons inside the modeled system, resulting in higher values of $k_{eff}$ through the fuel-cycle compared with the reference material. That makes the utilization of SiC cladding more favorable which has the highest excess reactivity, so the operating fuel cycle length is longer than the reference fuel-cladding system.

The results of thermal neutron spectra hardening for different types of cladding-fuel systems indicated that the FeCrAl cladding possessed larger absorption cross-sections than the Zr and SiC cladding. This resulted in spectrum hardening for the material with a larger cross-section and hence a higher amount of accumulated plutonium. The production of Pu-239 is higher in FeCrAl due to the hardening of neutron flux, as the fuel burnup continued toward the EOC.

Generally, both the Zr and SiC cladding exhibited similar neutronic behaviors. However, SiC is a better alternative candidate for the APR-1400 fuel-cladding system than FeCrAl due to the neutronics performance during the fuel life cycle. The use of SiC cladding slightly improved the neutron economy compared with the reference cladding, which might enhance the APR-1400 performance in terms of both economic and safety aspects. By contrast the FeCrAl fuel-cladding system indicated a significant neutronics penalty owing to the large cross-section for absorbing thermal neutrons. In the future, a sensitivity analysis will be performed to overcome the neutronics penalty associated with utilizing FeCrAl as an alternative cladding.

**Author Contributions:** Conceptualization, M.A. and S.A.A.; methodology, M.A.; software, M.A.; validation, S.A.A.; formal analysis, M.A.; investigation, M.A. and S.A.A.; resources, S.A.A.; data curation, M.A.; writing—original draft preparation, M.A. and S.A.A.; writing—review and editing, M.A. and S.A.A.; visualization, M.A.; supervision, S.A.A.; project administration, S.A.A.; funding acquisition, S.A.A. All authors have read and agreed to the published version of the manuscript.

**Funding:** This research was supported by the UAE Ministry of Education (CRPG-2019, Grant No.: 1570604539) and the Emirates Nuclear Technology Center (ENTC), Khalifa University of Science and Technology, UAE.

**Institutional Review Board Statement:** Not applicable.

**Informed Consent Statement:** Not applicable.

**Data Availability Statement:** Data associated with this research are available and can be obtained by contacting the corresponding authors.

**Conflicts of Interest:** The authors declare no conflict of interest.

## References

1. Snead, M.A.; Katoh, Y.; Koyanagi, T.; Singh, G.P. *SiC/SiC Cladding Materials Properties Handbook*; No. ORNL/TM-2017/385; Oak Ridge National Lab. (ORNL): Oak Ridge, TN, USA, 2017. [CrossRef]
2. Pasamehmetoglu, K.; Massara, S.; Costa, D.; Bragg-Sitton, S.; Moatti, M.; Kurata, M.; Iracane, D.; Ivanova, T.; Bischoff, J.; Delafoy, C.; et al. State-of-the-Art Report on Light Water Reactor Accident-Tolerant Fuels. 2018. Available online: http://inis.iaea.org/Search/search.aspx?orig_q=RN:50015394 (accessed on 2 February 2022).
3. Powers, J.J. Fully Ceramic Microencapsulated (FCM) Replacement Fuel for LWRs. 2013. Available online: http://www.osti.gov/contact.html (accessed on 2 February 2022).
4. Bragg-Sitton, S.M.; Carmack, J.; Goldner, F. *Evaluation Metrics Applied to Accident Tolerant Fuels*; No. INL/CON-14-32641; Idaho National Lab. (INL): Idaho Falls, ID, USA, 2014.
5. Youinou, G.J.; Sen, R.S. Impact of Accident-Tolerant Fuels and Claddings on the Overall Fuel Cycle: A Preliminary Systems Analysis. *Nucl. Technol.* **2017**, *188*, 123–138. [CrossRef]
6. Nguyen, X.H.; Jang, S.; Kim, Y. Impacts of an ATF Cladding on Neutronic Performances of the Soluble-Boron-Free ATOM Core. *Int. J. Energy Res.* **2020**, *44*, 8193–8207. [CrossRef]

7. Allen, P.L.; Ford, L.H.; Shennan, J.v. Nuclear Fuel Coated Particle Development in the Reactor Fuel Element Laboratories of the U.K. Atomic Energy Authority. *Nucl. Technol.* **1977**, *35*, 246–253. [CrossRef]
8. Schulten, R. The HTR with SiC-Technology. *Nucl. Eng. Des.* **1993**, *140*, 261–267. [CrossRef]
9. Chunhe, T.; Jie, G. Improvement in Oxidation Resistance of the Nuclear Graphite by Reaction-Coated SiC Coating. *J. Nucl. Mater.* **1995**, *224*, 103–108. [CrossRef]
10. Kim, B.G.; Choi, Y.; Lee, J.W.; Lee, Y.W.; Sohn, D.S.; Kim, G.M. Multi-Layer Coating of Silicon Carbide and Pyrolytic Carbon on UO2 Pellets by a Combustion Reaction. *J. Nucl. Mater.* **2000**, *281*, 163–170. [CrossRef]
11. Lippmann, W.; Knorr, J.; Nöring, R.; Umbreit, M. Investigation of the Use of Ceramic Materials in Innovative Light Water Reactor—Fuel Rod Concepts. *Nucl. Eng. Des.* **2001**, *205*, 13–22. [CrossRef]
12. Verrall, R.A.; Vlajic, M.D.; Krstic, V.D. Silicon Carbide as an Inert-Matrix for a Thermal Reactor Fuel. *J. Nucl. Mater.* **1999**, *274*, 54–60. [CrossRef]
13. Alrwashdeh, M.; Alameri, S.A. Preliminary Neutronic Analysis of Alternative Cladding Materials for APR-1400 Fuel Assembly. *Nucl. Eng. Des.* **2021**, *384*, 111486. [CrossRef]
14. Price, R.J. Properties of Silicon Carbide for Nuclear Fuel Particle Coatings. *Nucl. Technol.* **2017**, *35*, 320–336. [CrossRef]
15. Powers, J.J.; Brian, D.W. A Review of TRISO Fuel Performance Models. *J. Nucl. Mater.* **2010**, *405*, 74–82. [CrossRef]
16. Snead, L.L.; Nozawa, T.; Katoh, Y.; Byun, T.-S.; Kondo, S.; Petti, D.A. Handbook of SiC Properties for Fuel Performance Modeling. *J. Nucl. Mater.* **2007**, *371*, 329–377. [CrossRef]
17. Ott, L.J.; Robb, K.R.; Wang, D. Preliminary Assessment of Accident-Tolerant Fuels on LWR Performance during Normal Operation and under DB and BDB Accident Conditions. *J. Nucl. Mater.* **2014**, *448*, 520–533. [CrossRef]
18. George, N.M.; Terrani, K.; Powers, J.; Worrall, A.; Maldonado, I. Neutronic Analysis of Candidate Accident-Tolerant Cladding Concepts in Pressurized Water Reactors. *Ann. Nucl. Energy* **2015**, *75*, 703–712. [CrossRef]
19. Wu, X.; Kozlowski, T.; Hales, J.D. Neutronics and Fuel Performance Evaluation of Accident Tolerant FeCrAl Cladding under Normal Operation Conditions. *Ann. Nucl. Energy* **2015**, *85*, 763–775. [CrossRef]
20. Zinkle, S.J.; Terrani, K.A.; Gehin, J.C.; Ott, L.J.; Snead, L.L. Accident Tolerant Fuels for LWRs: A Perspective. *J. Nucl. Mater.* **2014**, *448*, 374–379. [CrossRef]
21. Terrani, K.A.; Zinkle, S.J.; Snead, L.L. Advanced Oxidation-Resistant Iron-Based Alloys for LWR Fuel Cladding. *J. Nucl. Mater.* **2014**, *448*, 420–435. [CrossRef]
22. Terrani, K.A.; Parish, C.M.; Shin, D.; Pint, B.A. Protection of Zirconium by Alumina- and Chromia-Forming Iron Alloys under High-Temperature Steam Exposure. *J. Nucl. Mater.* **2013**, *438*, 64–71. [CrossRef]
23. Younker, I.; Fratoni, M. Neutronic Evaluation of Coating and Cladding Materials for Accident Tolerant Fuels. *Prog. Nucl. Energy* **2016**, *88*, 10–18. [CrossRef]
24. Yamamoto, A.; Ikehara, T.; Takuya, I.T.O.; Etsuro, S.A. Benchmark Problem Suite for Reactor Physics Study of LWR Next Generation Fuels. *J. Nucl. Sci. Technol.* **2002**, *39*, 900–912. [CrossRef]
25. Alrwashdeh, M.; Alameri, S.A.; Alkaabi, A.K. Preliminary Study of a Prismatic-Core Advanced High-Temperature Reactor Fuel Using Homogenization Double-Heterogeneous Method. *Nucl. Sci. Eng.* **2020**, *194*, 163–167. [CrossRef]
26. Alameri, S.A.; Alrwashdeh, M. Preliminary Three-Dimensional Neutronic Analysis of IFBA Coated TRISO Fuel Particles in Prismatic-Core Advanced High Temperature Reactor. *Ann. Nucl. Energy* **2021**, *163*, 108551. [CrossRef]
27. Pham, H.; Kurata, M.; Steinbrueck, M. Steam Oxidation of Silicon Carbide at High Temperatures for the Application as Accident Tolerant Fuel Cladding, an Overview. *Thermo* **2021**, *1*, 151–167. [CrossRef]
28. Alraisi, A.; Yi, Y.; Lee, S.; Alameri, S.A.; Qasem, M.; Paik, C.-Y.; Jang, C. Effects of ATF Cladding Properties on PWR Responses to an SBO Accident: A Sensitivity Analysis. *Ann. Nucl. Energy* **2022**, *165*, 108784. [CrossRef]
29. Guo, D.; He, C.; Zang, H.; Zhang, P.; Ma, L.; Li, T.; Cao, X. Re-Evaluation of Neutron Displacement Cross Sections for Silicon Carbide by a Monte Carlo Approach. *J. Nucl. Sci. Technol.* **2015**, *53*, 161–172. [CrossRef]
30. Pritychenko, B.; Mughabghab, S.F. Neutron Thermal Cross Sections, Westcott Factors, Resonance Integrals, Maxwellian Averaged Cross Sections and Astrophysical Reaction Rates Calculated from the ENDF/B-VII.1, JEFF-3.1.2, JENDL-4.0, ROSFOND-2010, CENDL-3.1 and EAF-2010 Evaluated Data Libraries. *Nucl. Data Sheets* **2012**, *113*, 3120–3144. [CrossRef]
31. Mughabghab, S.F. Thermal Neutron Capture Cross Sections Resonance Integrals and G-Factors. IAEA. February 2003. Available online: https://www.osti.gov/etdeweb/biblio/20332542 (accessed on 2 February 2022).
32. Suh, J.-K.; Kim, Y.-H. Advisory Committee on Reactor Safeguards Review of Reactor for the APR1400 Design Certification. In Proceedings of the Transactions of the Korean Nuclear Society Spring Meeting, Jeju, Korea, 18–19 May 2017.
33. Kim, I.; Kim, D.-S. APR1400—Development Status and Design Features. United States: American Nuclear Society—ANS. Available online: http://inis.iaea.org/search/search.aspx?orig_q=RN:40044533 (accessed on 1 July 2020).
34. Alnoamani, Z.; Alameri, S.A.; Elsawi, M. Neutronic and Fuel Performance Evaluation of Accident Tolerant Fuel Concepts in APR1400 Reactor. *Trans. Am. Nucl. Soc.* **2018**, *118*, 1010–1013.
35. APR1400 Design Control Document Tier 2 Chapter 4 Reactor. December 2014. Available online: https://www.nrc.gov/docs/ML1500/ML15006A042.pdf (accessed on 1 July 2020).
36. Leppänen, J.; Pusa, M.; Viitanen, T.; Valtavirta, V.; Kaltiaisenaho, T. The Serpent Monte Carlo Code: Status, Development and Applications in 2013. *Ann. Nucl. Energy* **2015**, *82*, 142–150. [CrossRef]

37. Fridman, E.; Leppänen, J. On the Use of the Serpent Monte Carlo Code for Few-Group Cross Section Generation. *Ann. Nucl. Energy* **2011**, *38*, 1399–1405. [CrossRef]
38. Van der Marck, S.C. Benchmarking ENDF/B-VII.1, JENDL-4.0 and JEFF-3.1.1 with MCNP6. *Nucl. Data Sheets* **2012**, *113*, 2935–3005. [CrossRef]
39. Alrwashdeh, M. 239Pu Evaluation Comparison Study. *Ann. Nucl. Energy* **2018**, *118*, 313–316. [CrossRef]
40. Alrwashdeh, M.; Kan, W. U233 Data Evaluation for Criticality Study. *J. Nucl. Eng. Radiat. Sci.* **2016**, *2*, 034501. [CrossRef]
41. Leppänen, J. On the Use of Delta-Tracking and the Collision Flux Estimator in the Serpent 2 Monte Carlo Particle Transport Code. *Ann. Nucl. Energy* **2017**, *105*, 161–167. [CrossRef]
42. Hosokawa, T. Nuclear Fuel Element. Patent JPH03245090A, 31 October 1991. Available online: https://patents.google.com/patent/JPH03245090A/en?oq=Hosokawa%2c+Takanori.+(1990).+Nuclear+fuel+element+(JPH03245090A).+Japan (accessed on 2 February 2022).
43. Valtavirta, V.; Viitanen, T.; Leppänen, J. Internal Neutronics-Temperature Coupling in Serpent 2. *Nucl. Sci. Eng.* **2017**, *177*, 193–202. [CrossRef]